2011 IEEE International Conference on Robotics and Automation
Shanghai International Conference Center
May 9-13, 2011, Shanghai, China

Optically tracked multi-robot system for keyhole neurosurgery

Mirko Daniele Comparetti* Elena De Momi*† Alberto Vaccarella* Matthias Riechmann‡
Giancarlo Ferrigno*
*NearLab, Bioengineering Department, Politecnico di Milano, Milan, Italy
†ITIA, Consiglio Nazionale delle Ricerche, Milan, Italy
‡Institut für Prozessrechentechnik, Automation und Robotik, Karlsruher Institut für Technologie, Karlsruhe, Germany

***Abstract*— Robotic systems have been introduced in surgery to increase the intervention accuracy. In this framework, the ROBOCAST system is an optically controlled multi-robot chain aimed at enhancing the accuracy of surgical probe insertion during keyhole neurosurgery procedures. The system is composed by three robots, connected as a multiple kinematic chain (serial, parallel and linear) totaling 13 degrees of freedom (DoFs) and is it is used to automatically align the probe onto the desired trajectory.**

This paper presents an iterative approach for aligning the surgical probe with the planned target pose, reducing both the translation and the rotation errors. An experimental protocol was designed, in order to assess the system performances in terms of residual targeting errors and convergence ratio.

The proposed targeting procedures allows obtaining (0.06 ± 0.02) mm **and** $(0.8 \pm 0.2) \times 10^{-3}$ rad **as residual median errors, thus satisfying the operational requirements** (1 mm)**. The performances proved to be independent upon the robots calibration accuracy.**

I. INTRODUCTION

In keyhole neurosurgery, probes or electrodes (e.g. for biopsy, deep brain stimulation, stereo-EEG) are inserted into the brain through a small burr-hole in the skull. Robotic systems have been used to automatically position and insert such probes into the brain [1].

Passive systems autonomously move to a predefined position (e.g. the probe's entrance location) before locking and powering off. The probe is then manually inserted. Examples are Neuromate (Renishaw ltd., UK) and ROSA™ (MedTech, France) [2].

Semi-active robotic systems can be tele-operated, i.e. the surgeon interacts with the remote slave robot through a master handling device. In semi-active systems the probe is driven by actuators, such as in the NeuroArm, developed for microsurgery and stereotaxy brain procedures [3].

When using robots, the pre-operative plan and the patients images must be registered with the robot reference frame. To this aim, tracking systems are used for guiding the surgical robotic arm (for total hip replacement [4], for neurosurgery [5] and for bone ablation [6]). The integration of the robot and tracking systems requires a calibration procedure. Optical tracking systems, exploited for registration, were also used to further correct the position of the robot when deviations between the actual and the planned position are detected [7]. In robotic endoscopy applications, in order to decrease the noise in the signals provided by the tracking system and to correct possible robot inaccuracies, Kalman filters were applied to correct the position of the trochar point [8]. Kalman filters were also used for data fusion of redundant sensory information (from encoders and optical tracking systems) [9]. Tracking systems performances for robot control can be improved by the addition of inertial measurements units [10] in order to increase the control robustness with respect to marker occlusions, to compensate for delay of the optical system and to reduce noise.

The approach herein presented combines navigation and robotic assistance through three series connected robots for keyhole neurosurgery.

Serial robots have excellent repeatability, but their absolute positioning accuracy is low because of modeling errors in their kinematics. On the contrary, parallel robots have greater accuracy but they suffer of a limited workspace, if compared with their footprint. The multi-robot cell approach, having a large number of DoFs, allows performing the surgical task while optimizing the kinematic chain. Multi-robot approach for neurosurgery applications was already proposed in the Evolution I [11], designed for micro-neurosurgical and micro-endoscopic applications. A parallel kinematic machine (PKM) was coupled with an articulated mobile platform achieving 20 µm as positioning accuracy. The system was validated on six patients and then commercialized, but eventually the company failed.

In this paper we present the experimental results of a new control scheme for optical-controlled multi-robot targeting by using the ROBOCAST system as test-bench [12]. A biopsy probe is positioned by the modular robotic system at the entry point on the patient skull and then inserted in the brain via tele-operation control through an haptic device. In this approach, the optical tracking system allows iterative corrections of the pose of all the three robots, in case errors between the desired and the actual poses of the probe are detected. It also checks the overall system safety: whenever inconsistency is detected among the redundant sensors, the system raises a warning and blocks the advancement of the probe in the brain.

The paper is organized as follows: section II-A presents the ROBOCAST sensors and actuators; section II-B describes the spatial relations among internal robotic sensors

This work was supported by the EU Project Grant FP7-ICT-215190 ROBOCAST

(encoders) and external sensors (optical tracking); section II-C introduces the iterative targeting algorithms; section II-D presents the experimental protocol, and section II-E the metrics for performance evaluations. In section III and IV the results of the experiments are presented and discussed.

II. Materials and Methods

A. The robotic system

The ROBOCAST system is a robotic chain of three robots totalling 13 DoFs. As described in [12], the system encompasses (see Table I for details):

- the Gross Positioner, GP, (PathFinder, Prosurgics Ldt, UK); a serial 6 DoFs arm, which is used to approach the patient head [13];
- the Fine Positioner, FP, (MARS, Mazor, Israel); a parallel 6 DoFs PKM, used to further correct the targeting. It is rigidly connected to the GP via a quick release interlock;
- the Linear Actuator, LA; 1-DoF piezo-actuator, which makes the biopsy linear probe advance through a teleoperated haptic interface (Omega, Force Dimension, Switzerland) [14]. The LA is attached to the FP end effector (EE) upper plate.

The Certus optical tracking system (NDI, Ontario, Canada), with 0.15 mm stated accuracy, is used for surveying the overall robotic chain. Dynamical Reference Frames (DRFs), rigid bodies composed of four active markers each, are attached to all the bases and the end-effectors of the robots. The tracking system is interfaced with the ROBOCAST control system through the Sensor Manager, which is based on the IGSTK framework [16].

B. Spatial relations

In order to compute the spatial transformations between the robot internal sensors (encoders) and the optical tracking system, the approach described in [17] was used to calibrate both the GP and the FP. X_{GP}, Y_{GP}, X_{FP} and Y_{FP} represent the transformations between the DRFs in the optical reference frame and the robots internal reference frame (see Fig. 1), in particular:

- X_{GP} is the transformation between the GP end-effector and the origin of the DRF attached to the GP end-effector;
- Y_{GP} is the transformation between the GP base and the origin of the DRF attached to the GP base;
- X_{FP} is the transformation between the FP end-effector and the origin of the DRF attached to the FP end-effector;
- Y_{FP} is the transformation between the FP base and the origin of the DRF attached to the FP base.

To calibrate, the GP working volume was sampled acquiring 27 poses (in a sphere of 173.21 mm radius). In order to sample the FP working volume as well, 27 poses were acquired (in a sphere of 7.86 mm in radius).

In order to calibrate the LA, the probe was advanced for 50 mm (back and forth with 2 mm spacing) and 3D coordinates of the tip position sampled using a custom built divot

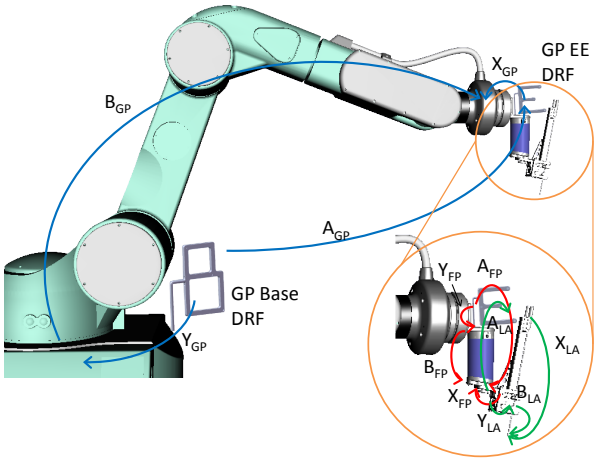

Fig. 1. Spatial transformations between the robots internal reference system and the three DRFs

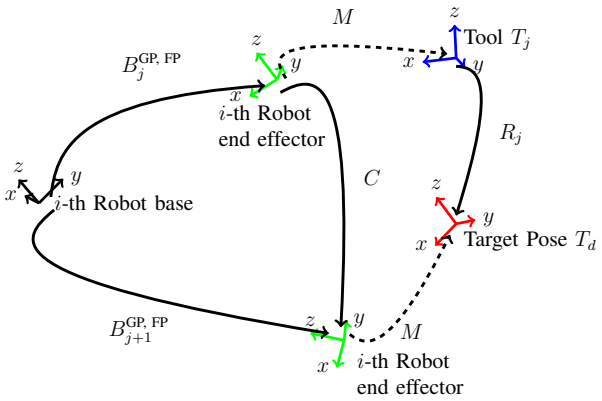

Fig. 2. Spatial transformations used during targeting. M is the spatial relation between the tool and the robot end-effector; for the GP robot it is $M = X_{\text{GP}}^{-1} \cdot X_{\text{FP}} \cdot B_{\text{GP}} \cdot X_{\text{FP}}^{-1} \cdot Y_{\text{LA}} \cdot B_{\text{LA}}$ and for the FP robot it is $M = X_{\text{FP}}^{-1} \cdot Y_{\text{LA}} \cdot B_{\text{LA}}$

DRF. Principal Component Regression was applied in order to compute the line approximating the probe advancement in the 3D space.

"Targeting" brings the probe tip T_j reference frame in the desired Target Pose T_d outside the patient skull as planned in the pre-operative phase (trochar position). From there, in the hypothesized surgical scenario, the probe is advanced by the surgeon by using the haptic interface [12].

In order for the T_j reference frame to reach the T_d, the i-th robot ($i = 1 \dots 2$) has to change its pose from B_j to B_{j+1} (Fig. 2).

If M represents the transformation between T_j and the i-th robot end-effector reference frame, the transformation to be applied to the i-th robot end effector C is:

$$C = M \cdot R_j \cdot M^{-1} \tag{1}$$

where R_j is the transformation between the PT reference frame and the Target Pose (T_d). Therefore the robot pose B_{j+1} is:

TABLE I

DESCRIPTION OF THE ROBOTS

ROBOT	Architecture	# DoFs	Accuracy	Velocity	Workspace
GP	serial	6	0.5 mm [15]	$50\,\mathrm{mm\,s^{-1}}$*	$(0.75 \times 0.75 \times 0.75)\,\mathrm{m^3}$*
FP	parallel	6	<0.1 mm	$1.3\,\mathrm{mm\,s^{-1}}$, $4.3\,^\circ\,\mathrm{s^{-1}}$	$(40 \times 40 \times 10)\,\mathrm{mm^3}$, $(12 \times 12 \times 12)^\circ$
LA	linear	1	8 µm	$2\,\mathrm{mm\,s^{-1}}$	110 mm

* Fixed by ROBOCAST specification

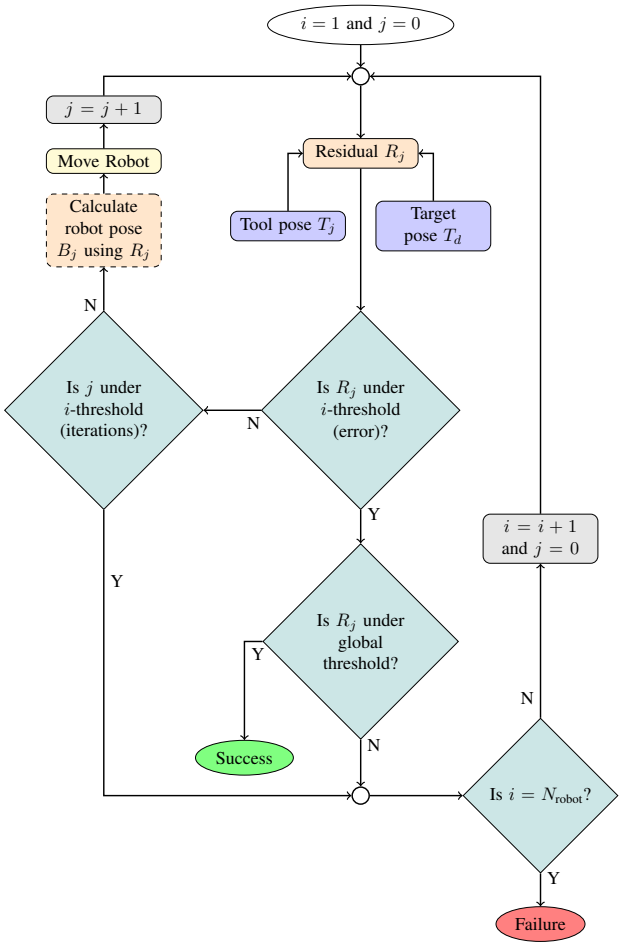

Fig. 3. Iterative corrections algorithm (i indices refer to robots and j indices refer to iteration numbers). Residuals (R_j) represents the error between the actual PT pose (T_j) and the Target Pose (T_d). Global threshold is the targeting threshold for the LA.

$$B_{j+1} = B_j \cdot C \tag{2}$$

C. The closed loop targeting algorithms

The translation error (T) has been defined as the Euclidean distance between the desired (T_d) and the actual (T_j) poses [18], while the rotation error is the first component of the quaternion (A) representing the rotation part of the transformation between T_d and T_j.

The targeting algorithm is described in Fig. 3: first the i-th robot approaches the target with an iterative approach until the error R_j (both the translation (T) and the rotations (A) components) is below a threshold (specifically defined for each robot) or if the maximum number of iterations is reached. Then the $(i+1)$-th robot is moved and the loop continues until success or failure are met.

The robot arm pose (dashed block represented in Fig. 3) was computed using two different approaches:

1) (*Total*) The i-th robot was moved in order to completely correct the residual transform R_j;
2) (*Sigmoid*) The R_j transform correction was reduced in magnitude in order to allow the robot to get closer to T_d, avoiding instabilities. The R_j translation component was scaled multiplying T times a value n computed as follows:

$$n\left(\dot{x}\right) = \frac{1}{1 + e^{\frac{\dot{x}}{10}}} \tag{3}$$

where $\dot{x}$ is the estimation of the error (Euclidean distance among T_j and T_d) first derivative, computed using finite differences method between subsequent iterations.

As an example, the *Sigmoid* correction n is 0.5 when the error is not changing from the previous iteration. When the error is decreasing, thus $\dot{x} < 0$, the correction n is close to 1, while if the error increases the correction n is reduced. The parameter $\frac{1}{10}$ of the *Sigmoid* was empirically chosen.

D. The experimental protocol

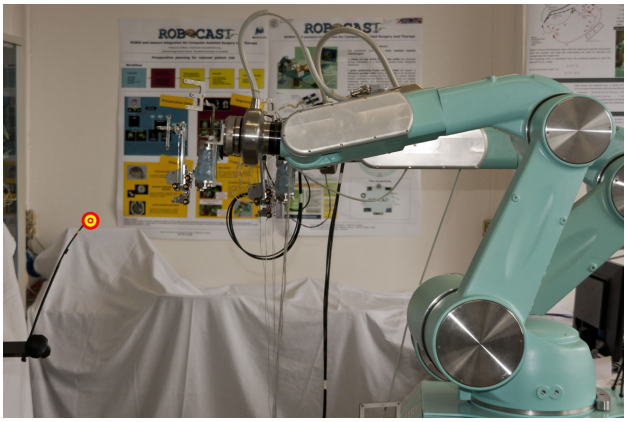

Fig. 4. Targeting set up; the red-and-yellow dot is the target.

As shown in Fig. 4, 22 Target Poses (T_d) were acquired in the working volume (in a sphere of 750 mm diameter), i.e. the operating theatre. Then the modular-robotic system

TABLE II
TEST PERFORMED

Test performed	*Targeting* *Targeting*_X_{GP} *Targeting*_X_{FP}
Number of trials	22
GP threshold	2 mm (*T*), 0.1 rad (*A*)
FP threshold	0.08 mm (*T*), 0.01 rad (*A*)
Maximum iteration per robot	10
Acquisition frequency	30 Hz

was moved in order to reach the Target Poses using the two algorithms described in § II-C. The test was named *Targeting*.

The GP threshold was set to 2 mm for translation (T) and 0.1 rad for rotation (A) with 10 iterations maximum allowed, after which the FP was moved towards the Target Pose. The FP threshold was set to 0.08 mm (corresponding to the expected accuracy of DRFs [19]) for translation and 0.01 rad for rotation with 10 iterations maximum.

In order to test the algorithm robustness, the calibration (§ II-B) was altered on purpose by multiplying the calibration matrix (X_{GP}) by transformation matrices randomly chosen in a population of (0-100) mm range of translation and (0-0.26) rad of rotation (uniform distribution); this test was named *Targeting*_X_{GP}. Another test was performed by multiplying the calibration matrix (X_{FP}) by transformation matrices randomly chosen in a population of (0-5) mm range of translation and (0-0.03) rad of rotation (uniform distribution). The test was named *Targeting*_X_{FP}. The test protocol is summarized in Table II.

For each targeting trial, all DRFs poses were acquired at 30 Hz.

E. Data analysis

In order to compare the overall targeting accuracy, the following metrics were computed:

- Residual Error (RE): Euclidean distance between the actual and the desired pose;
- Convergence Rate (CR): ratio between number of targeting under threshold ("Success" in Fig. 3) and all the trials (22).

The two algorithms (*Total* and *Sigmoid*) performances (RE and CR) were compared using non-parametric Kruskal-Wallis tests with $p < 0.05$ significance (STATISTICA, StatSoft).

III. RESULTS

Fig. 5a and Fig. 6a show the error decreasing during the iterations in the *Targeting* test. The GP approaches the Target Pose in the first iteration, from the second iteration the control is left to the FP by both the algorithms (RE is below the 1st robot threshold, 2 mm). While the *T* component of the RE converges almost monotonically towards the minimum, the *A* component is oscillating and can be unstable in case of *Total* correction (at iteration 7th and 8th). The *Sigmoid* algorithm has better performances in terms of CR (Fig. 7), but this is not statistical significant with respect to the *Total* algorithm. Even if better absolute performances were achieved in terms of *T* component of RE with the *Sigmoid* approach (0.05 ± 0.01) mm, no statistical significant difference is found (Fig. 8a). The angular component (*A*) of the RE is comparable, but the *Sigmoid* algorithm has a lower inter-quartile range (Fig. 8b).

Also in case the GP is mis-calibrated (*Targeting*_X_{GP}), from the second iteration the control is left to the FP by both the algorithms. The *Sigmoid* algorithm has slightly worse performances in terms of CR (Fig. 7), but this is not statistical significant with respect to the *Total* algorithm. Even if better absolute performances were achieved in terms of *T* component of RE with the *Total* approach (0.060 ± 0.015) mm, no statistical significant difference is found (Fig. 8a). Using the *Sigmoid* algorithm, the angular component (*A*) of the RE is lower and it is reached with a lower number of iterations (Fig. 8b and Fig. 6b).

In case the FP is mis-calibrated (*Targeting*_X_{FP}), the *Total* algorithm happened to require 10 iterations of GP corrections and the T component of the RE is not converging monotonically towards the minimum error. Differently, the GP exit the control loop after the first iteration with the *Sigmoid* algorithm. The *Sigmoid* algorithm has slightly better performances in terms of CR (Fig. 7), but this is not statistically significant with respect to the *Total* algorithm. Even if better absolute performances were achieved in terms of *T* component of RE with the *Total* approach, (0.05 ± 0.01) mm, no statistical significant difference is found (Fig. 8a). Using the *Sigmoid* algorithm, the angular component (*A*) of the RE is lower (Fig. 8b).

Comparing the same algorithms performances among different testing conditions, no statistical significant difference was found, either in terms of *T* component, or in term of *A* component.

IV. DISCUSSION

In this paper we show the experimental evaluation of a multi-robot system (three series connected robots) for keyhole neurosurgery. Kinematic redundancy allows optimizing the robot approach towards the patient. The miniaturized parallel robot (FP) mounted on the serial robot (GP) provides a more accurate surgical probe pose, due to its greater accuracy and resolution. In order to apply such an hybrid configuration to the operating room, a smaller and more compact system has to be designed in the future (i.e. a smaller gross positioner), but results reported here still hold.

With regards to targeting performances, it is worth recalling that the system was specially designed for keyhole approaches, where a straight surgical probe is inserted in the brain tissue and the robot acts as an assistant providing an accurate holder for guiding insertion. Therefore the aim of the study is to improve the accuracy of targeting in terms of position and rotation errors.

Two algorithms were developed and tested in order to optimize the targeting accuracy. The residual error, detected

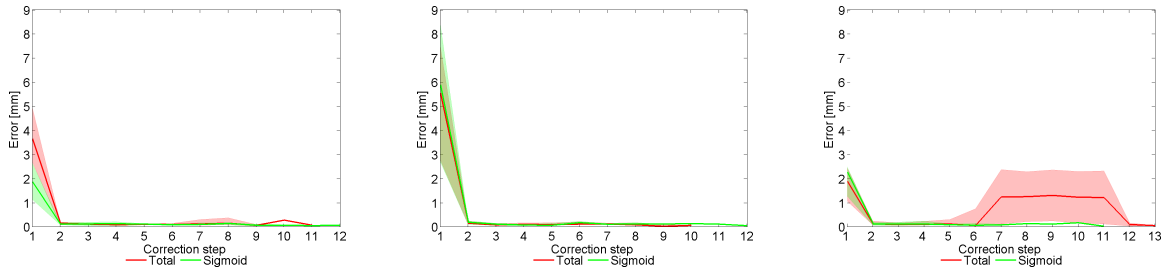

(a) *Targeting* (b) *Targeting*_X_{GP} (c) *Targeting*_X_{FP}

Fig. 5. Median values of R_j T component versus the iteration number. Quartiles ranges are also shown in case numerosity is greater than 1

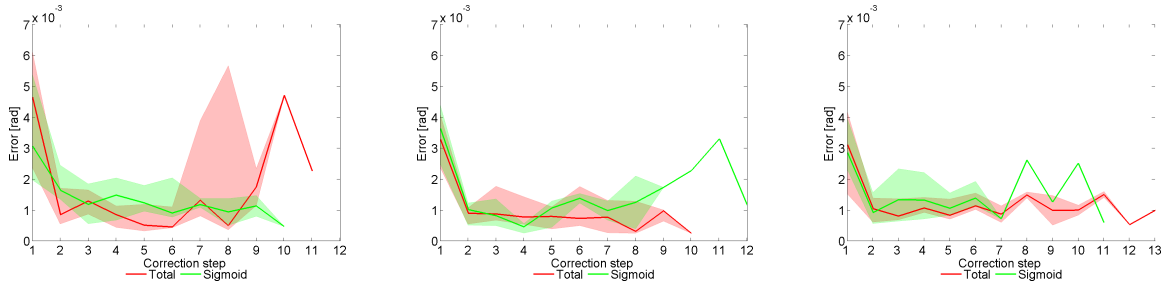

(a) *Targeting* (b) *Targeting*_X_{GP} (c) *Targeting*_X_{FP}

Fig. 6. Median values of R_j A component versus the iteration number. Quartiles ranges are also shown in case numerosity is greater than 1

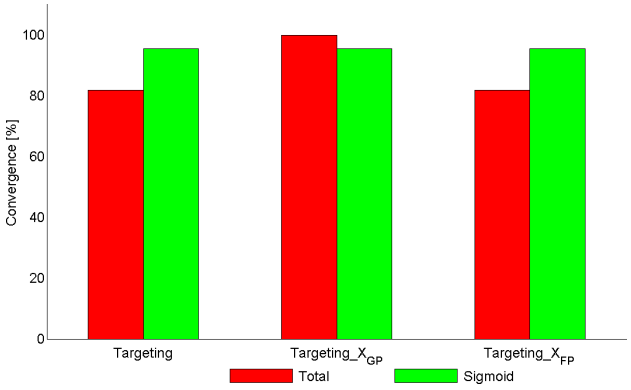

Fig. 7. CR performance indices

as difference from the actual pose of the tip of the surgical probe with respect to the desired position in the optical reference system, is corrected iteratively, first approaching with the gross positioner and then refining the targeting with the fine positioner, before leaving the control to the tele-operation modality. The optical feedback approach proposed by [8] allowed reaching (2.6 ± 0.8) mm as maximum error at the first iteration and (0.60 ± 0.36) mm as final targeting error, while [9] reached 0.5 mm of accuracy in 99.9 % of the cases, without previous calibration. Our approach proved to be independent from the calibration residuals: even if the calibration transformation is inaccurate, the iterative algorithm allows reaching comparable residual errors with the accurate calibrations for both the serial and the parallel robots.

The feedback control scheme is based on kinematics and does not take into account the dynamics of the system, but the low speed and the update at discrete times quite distant in time does not require it. Stability problems were tackled by modulating the correction amplitude with the *Sigmoid* algorithm. Also, the target is considered fixed since the patient head is framed in a head-ring.

Stated optical system accuracy is 0.15 mm, which is the worse 3D localization error. When using a 4 markers DRF, the target error in the center of mass is 0.08 mm [19]. When approaching the target, distortion and optical system calibration errors concurring to the accuracy are reduced, and only quantization errors of the linear CCD sensors remain.

The tracking system, which provides overall surveillance, allows also increasing the safety of the application since the consistency of the calibration loop, together with the visibility of all DRFs, is continuously checked at 10 Hz by a Safety Check (similarly to what proposed in [9]). Whenever inconsistency is detected, the probe advancement in the brain is stopped and the system placed in safe state.

Future work will be directed towards the optimization of the parameters of the *Sigmoid* function for error correction, e.g. to increase the correction in case the error is constant between two subsequent iteration steps without causing system oscillations.

REFERENCES

[1] G. Dogangil, B. L. Davies, and F. Rodriguez y Baena, "A review of medical robotics for minimally invasive soft tissue surgery," *Proceedings of the Institution of Mechanical Engineers, Part H: Journal of Engineering in Medicine*, vol. 224, no. H5, Sp. Iss. SI, pp. 653–679, 2010.

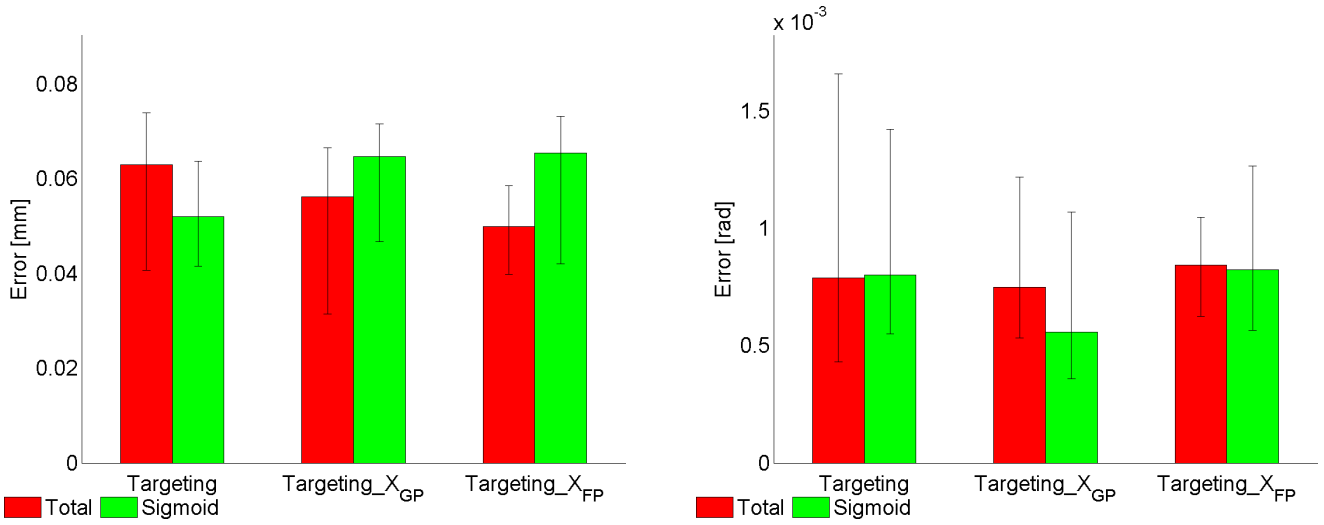

(a) T component

(b) A component

Fig. 8. RE components

[2] M. Cossu, G. Lo Russo, S. Francione, R. Mai, L. Nobili, I. Sartori, L. Tassi, A. Citterio, N. Colombo, M. Bramerio, C. Galli, L. Castana, and F. Cardinale, "Epilepsy surgery in children: Results and predictors of outcome on seizures," *Epilepsia*, vol. 49, no. 1, pp. 65–72, Jan. 2008.

[3] G. Sutherland, I. Latour, and A. Greer, "Integrating an image-guided robot with intraoperative mri: a review of the design and construction of NeuroArm." *IEEE engineering in medicine and biology magazine: the quarterly magazine of the Engineering in Medicine & Biology Society*, vol. 27, no. 3, p. 59, 2008.

[4] R. A. Castillo Cruces, H. Christian Schneider, and J. Wahrburg, *Medical Robotics*. I-Tech Education and Publishing, 2008, ch. Cooperative Robotic System to Support Surgical Interventions.

[5] T. Xia, C. Baird, G. Jallo, K. Hayes, N. Nakajima, N. Hata, and P. Kazanzides, "An integrated system for planning, navigation and robotic assistance for skull base surgery," *International Journal of Medical Robotics and Computer Assisted Surgery*, vol. 4, no. 4, pp. 321–330, Dec. 2008.

[6] J. Burgner, J. Raczkowsky, and H. Wörn, "End-effector calibration and registration procedure for robot assisted laser material processing: tailored to the particular needs of short pulsed co 2 laser bone ablation," in *Proceedings of the 2009 IEEE international conference on Robotics and Automation*. IEEE Press, 2009, pp. 2136–2141.

[7] J. Cornellà, O. Elle, W. Ali, and E. Samset, "Improving cartesian position accuracy of a telesurgical robot," in *IEEE International Symposium on Industrial Electronics, 2008. ISIE 2008*, 2008, pp. 1261–1266.

[8] J. Cornella, O. J. Elle, W. Ali, and E. Samset, "Intraoperative navigation of an optically tracked surgical robot," in *Medical Image Computing and Computer-Assisted Intervention - MICCAI 2008, PT II, proceedings*, ser. Lecture notes in Computer Science, D. Metaxas, L. Axel, G. Fichtinger, and G. Szekely, Eds., vol. 5242, 2008, pp. 587–594.

[9] S. Baron, H. Eilers, B. Munske, J. L. Toennies, R. Balachandran, R. F. Labadie, T. Ortmaier, and R. J. Webster, III, "Percutaneous inner-ear access via an image-guided industrial robot system," *Proceedings of the Institution of Mechanical Engineers, Part H: Journal of Engineering in Medicine*, vol. 224, no. H5, Sp. Iss. SI, pp. 632–648, 2010.

[10] A. Tobergte, F. Fröhlich, M. Pomarlan, and G. Hirzinger, "Towards accurate motion compensation in surgical robotics," in *Robotics and Automation (ICRA), 2010 IEEE International Conference on*. IEEE, 2010, pp. 4566–4572.

[11] M. Zimmermann, R. Krishnan, A. Raabe, and V. Seifert, "Robot-assisted navigated endoscopic ventriculostomy: implementation of a new technology and first clinical results," *Acta Neurochirurgica*, vol. 146, no. 7, pp. 697–704, 2004.

[12] E. De Momi and G. Ferrigno, "Robotic and artificial intelligence for keyhole neurosurgery: the ROBOCAST project, a multi-modal autonomous path planner," *Proceedings of the Institution of Mechanical Engineers, Part H: Journal of Engineering in Medicine*, vol. 224, no. 5, pp. 715–727, 2010.

[13] G. Deacon, A. Harwood, J. Holdback, D. Maiwand, M. Pearce, I. Reid, M. Street, and J. Taylor, "The pathfinder image-guided surgical robot," *Proceedings of the Institution of Mechanical Engineers, Part H: Journal of Engineering in Medicine*, vol. 224, no. 5, pp. 691–713, 2010.

[14] D. De Lorenzo, R. Manganelli, I. Dyagilev, A. Formaglio, E. De Momi, D. Prattichizzo, M. Shoham, and G. Ferrigno, "Miniaturized rigid probe driver with haptic loop control for neurosurgical interventions," in *Proceedings of the 2010 3rd IEEE RAS & EMBS International Conference on Biomedical Robotics and Biomechatronics, Tokyo, Japan*, 2010, pp. 522–527.

[15] M. Eljamel, "Validation of the PathFinder^{TM} neurosurgical robot using a phantom," *The International Journal of Medical Robotics and Computer Assisted Surgery*, vol. 3, no. 4, pp. 372–377, 2007.

[16] A. Vaccarella, P. Cerveri, E. De Momi, and G. Ferrigno, "A new IGSTK-based architecture for the integration of multimodal sensors and robots in neurosurgical robotics applications," in *Proceedings of the 24th International Congress and Exhibition*, vol. 5, June 2010, pp. 308–309.

[17] E. De Momi, P. Cerveri, E. Gambaretto, M. Marchente, O. Effretti, S. Barbariga, G. Gini, and G. Ferrigno, "Robotic alignment of femoral cutting mask during total knee arthroplasty," *International Journal of Computer Assisted Radiology and Surgery*, vol. 3, no. 5, pp. 413–419, 2008.

[18] S. Kumar, P. P, A. Dutta, and L. Behera, "Visual motor control of a 7DOF redundant manipulator using redundancy preserving learning network," *Robotica*, pp. 1–16, 2009.

[19] J. West and C. Maurer, "Designing optically tracked instruments for image-guided surgery," *IEEE Transactions on Medical Imaging*, vol. 23, no. 5, pp. 533–545, May 2004.